



Published in final edited form as:

*J Biomed Opt.* 2008 ; 13(5): 054042. doi:10.1117/1.2982535.

## Predicting In Vivo Fluorescence Lifetime Behavior of NIR Fluorescent Contrast Agents Using In Vitro Measurements

Walter J. Akers, Mikhail Y. Berezin, Hyeran Lee, and Samuel Achilefu\*

Optical Radiology Lab, Department of Radiology, Washington University School of Medicine, 4525 Scott Avenue, St. Louis, MO 63110

### Abstract

Fluorescence lifetime (FLT) information is complementary to intensity measurement and can be used to improve signal-to-background contrast and provide environment sensing capability. In this study, we evaluated the FLTs of eight near-infrared fluorescent molecular probes in vitro in various solvent mediums and in vivo to establish the correlation between the in vitro and in vivo results. Compared with other mediums, two exponential fitting of the fluorescence decays of dyes dissolved in aqueous albumin solutions accurately predicted the range of FLTs observed in vivo. We further demonstrated that the diffusion of NIR reporter from a dye-loaded gel can be detected by FLT change in mice as a model of controlled drug release. The mean FLT of the NIR probe increased as the dye diffused from the highly polar gel interior to the more lipophilic tissue environment. The two-point analysis demonstrates an efficient in vitro method for screening new NIR fluorescent reporters for use as FLT probes in vivo, thereby minimizing the use of animals for FLT screening studies.

### Keywords

optical imaging; fluorescence lifetime; near-infrared; controlled drug release; fluorescent dye; albumin

### 1 Introduction

Optical detection methods using organic fluorescent contrast agents are widely used in biomedical research from in vitro assays and microscopy to whole-animal preclinical imaging.<sup>1</sup> While steady-state fluorescence imaging (intensity vs. wavelength) is frequently used as optical detection technique, time-resolved fluorescence measurements are becoming popular in biological research because of advances in imaging techniques and increased commercial availability of economical lasers and electronic components.<sup>2-4</sup> Fluorescence lifetime (FLT) is an intrinsic property of fluorescent compounds and corresponds to the average amount of time the molecules spend in the excited state prior to emission of a photon. An advantage of FLT imaging lies in the high sensitivity of the FLT properties of organic dyes to their environment such as pH, polarity, viscosity, oxygen saturation, or protein binding. The insensitivity of FLT on the local dye concentration minimizes the detrimental effects of concentration artifacts, including photobleaching and dye decomposition. In addition, the FLT is less perturbed by light scattering,<sup>5, 6</sup> excitation intensity, or sample turbidity.<sup>7</sup> FLT imaging also allows multiplex resolution of probes that exhibit the same steady state optical properties (absorption and emission) with different FLT characteristics. Thus, multiple targeted agents can be resolved within the same living biological system that allows monitoring diverse

Address Correspondence to: Samuel Achilefu, PhD, Optical Radiology Lab, 4525 Scott Avenue, St. Louis, MO 63110, Telephone: 314-362-8599, Fax: 314-747-5191, achilefus@mir.wustl.edu.

physiological processes at the same time. Current instrumentation allows FLT resolution of less than 0.2 ns, which favors detection of small FLT changes.

FLT imaging microscopy and FLT endoscopy have utilized intrinsic tissue FLT data to assess differences in distribution of factors such as NADH and FADH and their oxidation state to correlate with pathologic changes or other biological processes.<sup>8</sup> In addition, FLT-sensitive fluorescent probes with light emission below 600 nm have been developed for more accurate sensing of oxygen, calcium and pH.<sup>4</sup> Although these probes may be adequate for cell studies, their relatively short emission wavelength confines their use to studies where the depth of light penetration is not a concern. Previous studies have shown that molecular probes that absorb and emit light in the near-infrared (NIR) range (700-900 nm) are best suited for in vivo imaging. Accordingly, our lab and others initiated studies to explore the potential of FLT imaging using NIR molecular probes in whole-animal optical imaging.<sup>9-15</sup> For example, we recently showed subtle FLT differences in mouse tumor versus liver using NIR tumor-specific agent<sup>10</sup> and demonstrated the use of the same excitation and emission parameters to separate signals from two different NIR molecular probes in an in vivo animal model.<sup>9</sup> The increased use of contrast-enhanced FLT imaging has prompted the need to adequately characterize the FLT properties of existing and new NIR fluorescent probes. Our previous study shows that NIR polymethine cyanine dyes, which are widely used for in vivo studies, have small but distinct FLT changes in mediums with different solvent polarity index.<sup>16</sup> Considering the heterogeneity within living tissues, similar FLT changes are expected in animals.

To minimize the number of animals used to screen the behavior of the FLT properties of these dyes in vivo, we explored the correlation of FLT changes in vitro with in vivo data. This will allow development of a high throughput in vitro model to predict the behavior and to sense normal and abnormal physiological by FLT changes in vivo. The FLTs of NIR probes in various solvents with different polarity index were compared to the in vivo data to develop a scale of FLT sensitivity. We found that the mean FLT in aqueous albumin solution was close to the maximum value of the FLT in vivo, while the minimum value was close to polar solutions such as water. We further demonstrated the utility of FLT imaging in a controlled drug-release model that releases a polymethine dye (cypate) from a gel. The measured mean FLT of cypate reflected the differences of environment polarity between the gel and mouse tissue.

## 2 Methods

### 2.1 Near-Infrared Imaging Agents

Near-infrared dyes indocyanine green (ICG), IR-820, IR-806, and 3,3'-diethylthiatricarbocyanine iodide (DTTCI) were purchased from Sigma-Aldrich (St. Louis, MO) and used without further purification. Cypate, LS-276, LS-277 and LS-288 were synthesized as described previously<sup>17-19</sup> and their photophysical properties were described elsewhere.<sup>16, 20</sup> Bovine serum albumin (BSA) was obtained from Sigma-Aldrich. Methanol, ethanol, acetone, dimethylsulfoxide (DMSO), methylene chloride (DCM), and chloroform were of spectroscopic grade quality and ultrapure water (Milli-Q, Millipore, Billerica, MA) was used throughout the study.

### 2.2 In Vitro Spectroscopic Measurements

BSA (50 mg) was dissolved in 1 mL of 0.01 M phosphate-buffered saline (PBS; Sigma-Aldrich) to obtain physiologic-relevant concentration of albumin in human plasma. The stock solutions of the dyes (50–100  $\mu$ M) in DMSO were stored at -20 °C in the dark. Aliquots were added to the appropriate solvents or BSA-PBS solution (1 mL) and vortexed for 1 min. To prevent inner filter effect, samples were further diluted with the appropriate organic solvent or PBS buffer to adjust the absorbance maximum between 0.1–0.3.

Absorbance spectra were recorded on Beckman Coulter DU 640 spectrophotometer (Fullerton, CA) and fluorescence steady-state spectra were recorded on Fluorolog III fluorometer (Horiba Jobin Yvon, Edison, NJ) with 720 nm excitation and 5 nm band slits. All measurements were conducted at room temperature. The FLTs were measured using time-correlated single-photon-counting (TCSPC) technique (Horiba) with 773 nm excitation source NanoLed® (impulse repetition rate 1 MHz) at 90° to the detector (Hamamatsu Photonics, Japan). For the FLT measurements, the absorbance of the working solutions was maintained below 0.15 at 773 nm excitation wavelength by dissolving the stock solutions in the appropriate solvents. The FLT of cypate-agarose gel was recorded in solid state using solid sample holder at about 45° to the path of light beam to avoid direct light reaching the detector. The angle was optimized with a blank agarose gel without cypate. The detector was set to 820 nm with a 20 nm bandpass. The electrical signal was amplified by TB-02 pulse amplifier (Horiba) fed to the constant fraction discriminator CFD (Philips, The Netherlands). The first detected photon was used as a Start signal by time-to-amplitude converter (TAC) and the excitation pulse triggered the Stop signal. The multichannel analyzer (MCA) recorded repetitive start–stop signals from the TAC and generated a histogram of photons as a function of time-calibrated channels (6.88 ps/channel) until the peak signal reached 10,000 counts. The FLT was recorded on a 50 ns scale. The instrument response function was obtained using Rayleigh scatter of Ludox-40 (0.03% in MQ water; Sigma-Aldrich) in a quartz cuvette at 773 nm emission. Decay analysis software (DAS6 v6.1; Horiba) was used for FLT calculations. The goodness of fit was judged by  $\chi^2$  values, Durbin–Watson parameters, as well as visual observations of fitted line, residuals, and autocorrelation function. Two-exponential analyses were normally used for data fitting, except where three-exponential decay equations were used to improve  $\chi^2$  for analysis in BSA solutions. When the FLT components with insignificant contribution (<3%) were discarded, the decays were reported as single or dual-component systems in the case of two- or three-exponential fit. For solution systems with two emitting species, such as the BSA solutions, the FLTs were calculated by the following equations:

$$I(t) = \sum_{i=1}^n A_i \exp(-t/\tau_i) \quad (1)$$

$$F_i = \frac{A_i \tau_i}{\sum_j A_j \tau_j} \quad (2)$$

where  $F_i$  is the fractional component (%),  $\tau_i$  is the FLT (ns),  $A_i$  is the amplitudes, and  $n$  is 2 for two exponential model. Fitting of fluorescence decays with a single exponential model ( $n=1$ ) was used to report the average FLT.

### 2.3 Animal Treatment

All animal studies were performed in compliance with the Washington University School of Medicine Animal Studies Committee requirements for the humane care and use of laboratory animals in research. For in vivo NIR probe FLT measurement, male NCR nude mice were anesthetized and maintained with isoflurane gas (2% v/v) for fluorescent agent administration and imaging. Contrast agents dissolved in 100  $\mu$ L of 20% DMSO were injected via lateral tail vein. Concentrations were based on absorbance at 780 nm equivalent to 60  $\mu$ M cypate. For imaging of subcutaneously implanted cypate-loaded agarose gels, mice were anesthetized and maintained with isoflurane gas (2% v/v). A 5-mm incision was made through the skin flank region and a pocket made in the subcutaneous tissue by blunt dissection. A 0.5 mm<sup>3</sup> slab (1

×1 mm square by 0.5 mm thick) of 1% agarose gel containing 60 μM cypate was inserted into the pocket and the incision was closed with tissue adhesive. Gels were positioned such that the incision lay on the lateral aspect, with uninterrupted skin over the gel surface.

## 2.4 Imaging Method and Analysis

In vivo mouse images were acquired with a time-domain diffuse optical imaging system (eXplore Optix, ART, Inc. Montreal, Canada). The system produced excitation light via 780 nm, 80 MHz pulsed diode laser and captured emitted photons by fast photomultiplier tube with 830 nm telecentric emission filter. The detection system included a time-correlated single-photon counting device for in vivo fluorescence decay recording. The focal points of excitation and emission detection were separated by 3 mm to detect diffusely scattered fluorescence photons. Diffuse optical imaging improves depth resolution relative to reflectance imaging.<sup>21</sup> FLT imaging in live mice was performed as reported previously.<sup>9, 10</sup> Briefly, the animals were positioned on the heated imaging platform and a 2D scanning region of interest (ROI) was selected by top-view CCD camera to include the area from the neck to the pelvis. The 780 nm pulsed diode laser was set to 0.4 μW for excitation scans and adjusted for optimal signal strength, in the range 5-70 μW for fluorescence detection. ROI were raster-scanned in 1.5 mm increments for the controlled drug release (CDR) model and 3 mm increments for contrast agent imaging with 0.3 s integration time per pixel. Fluorescence data were acquired 0.5 to 2.5 hours after agent injection. Acquired images were analyzed with the OptiView software provided by ART, Inc. Data were reported as fluorescence intensity or FLT maps with each pixel representing the integration or curve fitting of the acquired temporal point-spread function (TPSF), respectively, at each detection point. Pixels with less than  $1 \times 10^5$  photon counts per second were not included in FLT measurement due to insufficient signal. In vivo FLT maps are displayed after fitting a single exponential decay function for simplicity. To determine the best model for in vivo FLT results, FLT values from different solvent models were compared to the average FLT values in the liver region from in vivo imaging. The liver region was chosen for data sampling as most agents accumulated in this organ nonspecifically relative to other tissues.

## 2.5 Statistical Analysis

Column statistics were performed to assess the correlation of in vitro and in vivo FLT measurements. Percent differences were calculated for each in vitro model relative to the reference model to assess the ability of each solvent system to predict in vivo FLT behavior. The percent differences were compared to assess the agreement of each in vitro model in relation to the in vivo FLT measurements. All analyses were performed using Prism 4.0 (GraphPad Software, San Diego, CA).

## 3 Results

### 3.1 Chemistry

NIR molecular probes synthesized in our lab and from commercial sources used in this study are shown in Fig. 1. All compounds are based on heptamethine dyes that differ in the nature of the heterocyclic end groups or substituents at the meso-position. The linear heptamethine dye cypate was prepared in high yield (>60%) from the reaction of glutaconaldehyde and the propanoic acid derivative of benzoindole, as reported previously.<sup>17, 22</sup> The meso-substituted dyes were prepared by a modified Suzuki coupling method.<sup>18</sup> The purity of all prepared compounds was determined by HPLC and LC-MS analyses. The choice of the dyes was based on several criteria. First, the dyes were selected to represent a broad range of FLT from 0.49 ns for IR-820 to 1.14 ns for DTTCI in albumin. Second, the probes were selected to represent different degrees of hydrophilicity determined by a number of sulfate groups in the molecule. For example, cypate with no sulfonate groups was sparingly insoluble in water, while LS-288

with four sulfonate groups was highly water soluble. Third, the synthesized dyes were designed to possess a reactive functionality (here, the carboxylic acid group) for labeling biomolecules such as peptides and proteins.

### 3.2 Comparison of In Vitro and In Vivo FLT of Molecular Probes

The spectral properties of the dyes were determined in solvents with different solvent polarity to explore the FLT behavior in different environment, as reported previously.<sup>16</sup> In these solvents, all of the dyes absorbed and emitted light in the NIR region (700-900 nm). The dyes also exhibit relatively small bathochromic absorption and emission shifts (5-30 nm) in high polarity relative to low polarity solvents, which is typical of heptamethine dyes.<sup>16</sup> In contrast, the dynamic emission spectra show significant solvent-dependent changes in FLT values (Table 2). The FLT changes correlated with the solvent polarity function, such as solvent orientation polarizability,  $\Delta f$ . In general, the FLT showed a decrease from low to high polarity solvents (from low to high values of  $\Delta f$ ). The fluorescence decays in most solvents were mono-exponential (>95% fractional contribution from the major component constituted the two exponential analysis), suggesting the presence of one major form of the emitter in solution (Table 1). This indicates the homogeneity of the solutions, albeit with polarity-dependent FLT in different solvents.

We also examined the FLT properties of the dyes in albumin, a major transport protein in blood. The average FLT of single exponential decay fits are shown in Table 1. According to molecular modeling studies,<sup>20</sup> albumin offers at least two binding pockets with significantly different polarities for the binding of heptamethine molecules. As a result, the molecular probes bound to albumin could exist in two different microenvironments that exhibit two distinct FLT with corresponding fractional contributions. In contrast to the single exponential decays found in organic solutions, the fluorescence decays in albumin solutions show a two exponential decay, revealing the presence of the two light-emitting states, except for DTTCI (Table 2).

For in vivo FLT study, mice were imaged after intravenous injection of individual dyes. The resulting FLT maps of the dyes were relatively flat compared with the intensity images, indicating the poor dependence of FLT on the dye concentration (Fig. 2).

Each compound tested demonstrated relatively distinct FLT ranging from 0.53 to 1.12 ns. The mean in vivo FLT measured from the liver region for different dyes are shown in Table 1 and reflect the general trend that fluorescent probes with longer FLT in vitro in any given solvent typically show longer FLT in vivo. An exception to the relatively flat FLT trend is the heterogeneous fluorescence intensity and FLT maps of LS-288 in mice (Fig. 3). The distinct short FLT in the bladder (0.70 ns) relative to other parts of the body (1.12 ns) was observed, indicating the water-rich environment in the urine (Table 3). The hydrophilic characteristics of the dye resulted in significant renal clearance relative to the more hydrophobic dyes used in this study.

Our results show that the dye FLT in albumin solutions best approximates the in vivo range of FLT as measured from the liver region. A graphical box and whiskers plot of this analysis is shown in Fig. 4. Two-exponential fitting of the acquired TPSFs for dyes in albumin solutions reliably predicted the range of FLT observed in vivo, with the largest deviations from the mean (mono-exponential fitting) in vivo measurements apparently due to differences in protein binding fractions (Table 2). FLT values for compounds in aqueous albumin solution showed the lowest bias relative to other solvents with an average difference of 0.7%.

### 3.2 Agarose Gel Implant FLT Imaging

Having demonstrated the potential to predict the *in vivo* behavior of NIR dyes in various mediums, we explored the use of FLT changes to monitor the release of encapsulated dyes *in vivo*. We used agarose gel implant containing cypate as a model of controlled drug release for this study. The site of surgery did not swell or show significant signs of inflammation during the imaging period, nor did the mice show signs of irritation or pain from the implant. High fluorescence intensity was measured from the area of the gel implant with significant fluorescence detected from the area surrounding the gel. We also detected fluorescence from the contralateral liver and kidney regions by 3 hours post-implant, demonstrating rapid cypate diffusion and absorption into systemic circulation (Fig. 5a). The measured FLT in the tissue surrounding the gel was substantially higher at several millimeters from the gel relative to the FLT of cypate in the agarose gel (Fig. 5b) with a near linear increase over distance from the gel center (Fig. 5c). “Because cypate is cleared from the body through hepatobiliary pathway, it is also possible that the stomach and intestines contributed some of the detected fluorescence in the liver and kidney regions.”

## 4 Discussion

FLT imaging is a versatile approach to study physiological and molecular processes.<sup>23-30</sup> The *in vivo* applications of FLT imaging using exogenous molecular probes require a clear understanding of the *in vivo* FLT properties of various dyes to delineate imaging artifacts from real signals. This is particularly important when using exogenous contrast agents capable of altering their FLT. Although the FLT properties of many visible fluorescent proteins and dyes are well documented, those of NIR molecular probes are not readily available. Recently, our lab and others have mapped the FLT of NIR dyes in animals.<sup>9, 10, 14</sup> In one study, we showed that the FLT of a tumor-specific molecular probe exhibited small FLT differences in the tumor and the liver.<sup>10</sup> A more recent study demonstrated our ability to separate the distribution of two NIR fluorescent probes in the same animal based on their FLT.<sup>9</sup> Other labs have developed a tomographic approach for high resolution FLT imaging in small animals.<sup>11, 13, 31</sup> With the availability of these instruments and diverse NIR molecular probes, it is only a matter of time before a surge in their *in vivo* use becomes a reality.

However, minimization of the number of animals needed to evaluate the FLT properties of new molecular probes *in vivo* would be facilitated by developing *in vitro* model to predict the FLT properties of these dyes. We recently demonstrated the high sensitivity of the FLT to the polarity of the mediums for heptamethine NIR fluorescent probes.<sup>16</sup> There are four major decay pathways for these cyanine dyes from the singlet excited state to the ground state: (1) radiative fluorescence process and three non-radiative pathways that include (2) internal conversion, (3) intersystem crossing, and (4) photoisomerization. Generally, photoisomerization decay pathway is solvent-dependent, while the internal conversion is a solvent-independent process. Polar solvents facilitate the mobility of the bonds in the excited state, diverting the energy from radiative to non-radiative pathway that results in shorter FLT. Although we established a correlation between the solvent polarity function and FLT by determining the dye FLT in various solvents, a correlation between *in vitro* and *in vivo* data is required to help interpret *in vivo* FLT images. This calls for the development of an *in vitro* system for high throughput screening of NIR probes for *in vivo* use, thereby minimizing the number of animals used for such screening studies.

Although many factors could affect FLT, we focused this study on solvent effects to reflect FLT behavior in the heterogeneous tissue environment. In general, the FLT of the NIR dyes examined do not respond significantly to changes in ion concentrations or pH within physiological relevant range. From the *in vitro* data obtained using a number of NIR molecular probes, we have demonstrated that the different FLT *in vivo* depend on the nature of the

molecular probe. In general, dyes with longer FLT in any given solvent generally exhibited longer FLT values in vivo. Data analysis of FLTs in various mediums identified albumin solution as a consensus model for predicting the in vivo FLT relative to the other mediums. This finding is supported by the fact that cyanine dyes are rapidly opsonized by plasma proteins such as serum albumin soon after injection.<sup>32</sup> Thus, a majority of the FLT values observed in vivo reflected the FLT of NIR dyes bound to serum albumin. In a two-component analysis, this correlation could be extended to a FLT-polarity scale, where the longest and shortest FLTs observed in vivo correlates with FLTs of the NIR dyes bound to albumin and in water, respectively. An interesting finding is the difference in the FLT of albumin-bound (liver) versus albumin-free (bladder) NIR dye, LS 288 (Fig. 3). In the hydrophilic bladder, the FLT (0.70 ns) is between that of water and methanol but the FLT in the liver is comparable to a value between ethanol and DMSO (Table 1). Comparison of the albumin/liver FLT to that of relatively protein-free urine (Table 3) suggests that the glomerular filtration mechanism of the kidney actively stripped the albumin of the dye, thereby excreting the free hydrophilic dye into the urine. A similar observation was not found for the relatively lipophilic dyes used in this study, which were excreted predominantly in the liver. The possible effect of the DMSO formulation on the in vivo FLT of dyes was not evaluated but based on other studies, this effect is expected to be negligible.

To further illustrate the utility of FLT imaging for monitoring controlled dye release in vivo, agarose gels containing cypate were subcutaneously implanted in the flank region of nude mice. As we described previously, the FLT of cypate is sensitive to differences in medium polarity but less sensitive to its viscosity.<sup>16</sup> Thus the short FLT of cypate inside the gel (0.3 ns) reflects the presence of a large amount of water molecules trapped inside the bundles of double helices formed by agarose molecules upon gelation.<sup>33</sup> Indeed, this value is close to the FLT of cypate in water (0.2 ns). The slightly larger FLT value in the gel than in pure water indicates the small contribution of viscosity or reflects a modification of the water polarity due to self-assembling of trapped water molecules inside the gel microcavities (Fig. 6).<sup>34</sup>

The FLT imaging showed that cypate diffuses out of the agarose gel into the more lipophilic subcutaneous space where it is absorbed into the systemic circulation and bound by plasma proteins, specifically albumin. Further, through a cascade of biological events, the albumin released the dye to the kidneys, which subsequently drained to the bladder. These physiological processes are reflected in the progressive FLT decrease from the liver and circulating blood to the water-rich environment of the kidneys and the bladder, which is similar to the aqueous interior of the gel. The linearity of the FLT increase with distance from the gel center is likely due to the diffuse nature of optical sampling, smoothing the expected exponential diffusion function. Each pixel represents a diffuse spectroscopic measurement that includes the 3 mm region separating the source and detector. These results show that the release and delivery of fluorescent agents from implanted controlled drug release devices can be assessed by FLT imaging. The status of regional tissue physiology may also be investigated non-invasively with FLT-sensitive fluorescent probes that are administered systemically. Therefore, the FLT map complements the fluorescence intensity image by providing functional and quantifiable information about tissue physiology. FLT contrast can also aid optical imaging methods by improving 3D localization.<sup>11, 31, 35</sup>

## 5 Conclusion

FLT imaging adds complimentary information to contrast-enhanced fluorescence intensity imaging. Using a number of NIR FLT-sensitive fluorescent probes in different solvents, we established a scale which is useful for evaluation the biological events derived from in vivo FLT imaging. In the case of polymethine probes, the scale is based on polarity functions of the surrounding media. The shortest FLT maps in vivo reflect the areas with highest polarities

similar to water, while the long FLT's correspond to more hydrophobic environment mostly due to uptake by hydrophobic pockets of plasma proteins. We showed that the longest FLT in vivo correlated with the FLT in albumin rather than to any other solvents. The use of organic and aqueous mediums to predict in vivo FLT's of dyes will facilitate the evaluation of new NIR dyes by in vitro method, thus reducing the number of animals needed to screen agents for full characterization of biological utility. To illustrate the utility of the developed FLT scale, we imaged the release of cypate from agarose gel to assess the feasibility of using FLT maps for modeling controlled release of drugs and contrast agents. The results showed that the mean FLT of cypate substantially increased as the dye diffused from the gel interior to the surrounding tissue, indicating the change in the dye environment from a highly polar gel core to the less polar tissue compartments of plasma proteins and subsequently to hydrophilic aqueous pockets of the kidneys and urine. The results show that some biological events not available from fluorescent intensity images can be monitored directly from the FLT map. This study illustrates the potential of using FLT imaging to monitor physiological processes at different parts of the body and opens many other opportunities in optical imaging.

## Acknowledgments

The authors thank Anthony Agee for technical assistance in animal imaging and Yunpeng Ye for providing a sample of cypate. This research was supported in part by the National Institutes of Health grants R01 CA109754, R01 EB1430, R33 CA100972, and R24 CA83060.

## References

1. Ntziachristos V. Fluorescence molecular imaging. *Annu Rev Biomed Eng* 2006;8:1–33. [PubMed: 16834550]
2. Elson D, Requejo-Isidro J, Munro I, Reavell F, Siegel J, Suhling K, Tadrous P, Benninger R, Lanigan P, McGinty J, Talbot C, Treanor B, Webb S, Sandison A, Wallace A, Davis D, Lever J, Neil M, Phillips D, Stamp G, French P. Time-domain fluorescence lifetime imaging applied to biological tissue. *Photochem Photobiol Sci* 2004;3(8):795–801. [PubMed: 15295637]
3. Suhling K, French PM, Phillips D. Time-resolved fluorescence microscopy. *Photochem Photobiol Sci* 2005;4(1):13–22. [PubMed: 15616687]
4. Tadrous PJ. Methods for imaging the structure and function of living tissues and cells: 2. Fluorescence lifetime imaging. *J Pathol* 2000;191(3):229–234. [PubMed: 10878542]
5. Cerussi AE, Maier JS, Fantini S, Franceschini MA, Mantulin WW, Gratton E. Experimental verification of a theory for the time-resolved fluorescence spectroscopy of thick tissues. *Appl Opt* 1997;36(1):116–124. [PubMed: 18250652]
6. Kuwana E, Sevick-Muraca EM. Fluorescence lifetime spectroscopy in multiply scattering media with dyes exhibiting multiexponential decay kinetics. *Biophys J* 2002;83(2):1165–1176. [PubMed: 12124296]
7. Ntziachristos V, Weissleder R. Charge-coupled-device based scanner for tomography of fluorescent near-infrared probes in turbid media. *Med Phys* 2002;29(5):803–809. [PubMed: 12033576]
8. Lakowicz JR, Szmacinski H, Nowaczyk K, Johnson ML. Fluorescence lifetime imaging of free and protein-bound NADH. *Proc Natl Acad Sci U S A* 1992;89(4):1271–1275. [PubMed: 1741380]
9. Akers W, Lesage F, Holten D, Achilefu S. In vivo resolution of multiexponential decays of multiple near-infrared molecular probes by fluorescence lifetime-gated whole-body time-resolved diffuse optical imaging. *Mol Imaging* 2007;6(4):237–246. [PubMed: 17711779]
10. Bloch S, Lesage F, McIntosh L, Gandjbakhche A, Liang K, Achilefu S. Whole-body fluorescence lifetime imaging of a tumor-targeted near-infrared molecular probe in mice. *J Biomed Opt* 2005;10(5):54003.
11. Godavarty A, Sevick-Muraca EM, Eppstein MJ. Three-dimensional fluorescence lifetime tomography. *Med Phys* 2005;32(4):992–1000. [PubMed: 15895582]



12. Hassan M, Riley J, Chernomordik V, Smith P, Pursley R, Lee SB, Capala J, Gandjbakhche AH. Fluorescence lifetime imaging system for in vivo studies. *Mol Imaging* 2007;6(4):229–236. [PubMed: 17711778]
13. Nothdurft, RE.; Patwardhan, SV.; Akers, WJ.; Achilefu, S.; Culver, JP. Biomedical Optics/Digital Holography and Three-Dimensional Imaging/Laser Applications to Chemical, Security and Environmental Analysis on CD-ROM. The Optical Society of America; Washington, DC: 2008. Fluorescence Lifetime Tomography for Whole Body Small Animal Imaging. BWE2
14. Abulrob A, Brunette E, Slinn J, Baumann E, Stanimirovic D. In vivo time domain optical imaging of renal ischemia-reperfusion injury: discrimination based on fluorescence lifetime. *Mol Imaging* 2007;6(5):304–314. [PubMed: 18092515]
15. Reynolds JS, Troy TL, Mayer RH, Thompson AB, Waters DJ, Cornell KK, Snyder PW, Sevick-Muraca EM. Imaging of spontaneous canine mammary tumors using fluorescent contrast agents. *Photochem Photobiol* 1999;70(1):87–94. [PubMed: 10420847]
16. Berezin MY, Lee H, Akers W, Achilefu S. Near infrared dyes as lifetime solvatochromic probes for micropolarity measurements of biological systems. *Biophys J* 2007;93(8):2892–2899. [PubMed: 17573433]
17. Achilefu S, Dorshow RB, Bugaj JE, Rajagopalan R. Novel receptor-targeted fluorescent contrast agents for in vivo tumor imaging. *Invest Radiol* 2000;35(8):479–485. [PubMed: 10946975]
18. Lee H, Mason JC, Achilefu S. Heptamethine cyanine dyes with a robust C-C bond at the central position of the chromophore. *J Org Chem* 2006;71(20):7862–7865. [PubMed: 16995699]
19. Mason, JC. Chemistry. Georgia State University; Atlanta, GA: 2001. The Synthesis of Novel Near-Infrared Heptamethine Cyanine Dyes.
20. Berezin MY, Lee H, Akers W, Nikiforovich G, Achilefu S. Ratiometric Analysis of Fluorescence Lifetime for Probing Binding Sites in Albumin with Near-Infrared Fluorescent Molecular Probes. *Photochem Photobiol* 2007;83:1–8.
21. Yodh A, Chance B. Spectroscopy and Imaging with Diffusing Light. *Phys Today* 1995;48(3):34–40.
22. Ye Y, Li WP, Anderson CJ, Kao J, Nikiforovich GV, Achilefu S. Synthesis and characterization of a macrocyclic near-infrared optical scaffold. *J Am Chem Soc* 2003;125(26):7766–7767. [PubMed: 12822971]
23. Dowling K, Dayel MJ, Lever MJ, French PM, Hares JD, Dymoke-Bradshaw AK. Fluorescence lifetime imaging with picosecond resolution for biomedical applications. *Opt Lett* 1998;23(10):810–812. [PubMed: 18087350]
24. Cubeddu R, Canti G, Pifferi A, Taroni P, Valentini G. Fluorescence lifetime imaging of experimental tumors in hematoporphyrin derivative-sensitized mice. *Photochem Photobiol* 1997;66(2):229–236. [PubMed: 9277142]
25. Cubeddu R, Canti G, Taroni P, Valentini G. Time-gated fluorescence imaging for the diagnosis of tumors in a murine model. *Photochem Photobiol* 1993;57(3):480–485. [PubMed: 8475182]
26. Lakowicz JR, Szmajcinski H, Nowaczyk K, Berndt KW, Johnson M. Fluorescence lifetime imaging. *Anal Biochem* 1992;202(2):316–330. [PubMed: 1519759]
27. Tadrous PJ, Siegel J, French PM, Shousha S, Lalani el N, Stamp GW. Fluorescence lifetime imaging of unstained tissues: early results in human breast cancer. *J Pathol* 2003;199(3):309–317. [PubMed: 12579532]
28. Andersson-Engels S, Canti G, Cubeddu R, Eker C, af Klinteberg C, Pifferi A, Svanberg K, Svanberg S, Taroni P, Valentini G, Wang I. Preliminary evaluation of two fluorescence imaging methods for the detection and the delineation of basal cell carcinomas of the skin. *Lasers Surg Med* 2000;26(1):76–82. [PubMed: 10637006]
29. Gandjbakhche AH, Chernomordik V, Hattery D, Hassan M, Gannot I. Tissue characterization by quantitative optical imaging methods. *Technol Cancer Res Treat* 2003;2(6):537–551. [PubMed: 14640765]
30. Schweitzer D, Hammer M, Schweitzer F, Anders R, Doebbecke T, Schenke S, Gaillard ER, Gaillard ER. In vivo measurement of time-resolved autofluorescence at the human fundus. *J Biomed Opt* 2004;9(6):1214–1222. [PubMed: 15568942]

31. Kumar ATN, Raymond SB, Boverman G, Boas DA, Bacskai BJ. Time resolved fluorescence tomography of turbid media based on lifetime contrast. *Opt Express* 2006;14(25):12255–12270. [PubMed: 19529654]
32. Cherrick GR, Stein SW, Leevy CM, Davidson CS. Indocyanine green: observations on its physical properties, plasma decay, and hepatic extraction. *J Clin Invest* 1960;39:592–600. [PubMed: 13809697]
33. Arnott S, Fulmer A, Scott WE, Dea ICM, Moorhouse R, Rees DA. The agarose double helix and its function in agarose gel structure. *J Mol Biol* 1974;90(2):269–272. [PubMed: 4453017]
34. Ratajska-Gadomska B, Gadomski W. Water structure in nanopores of agarose gel by Raman spectroscopy. *J Chem Phys* 2004;121(24):12583–12588. [PubMed: 15606280]
35. Hall D, Ma G, Lesage F, Wang Y. Simple time-domain optical method for estimating the depth and concentration of a fluorescent inclusion in a turbid medium. *Opt Lett* 2004;29(19):2258–2260. [PubMed: 15524373]

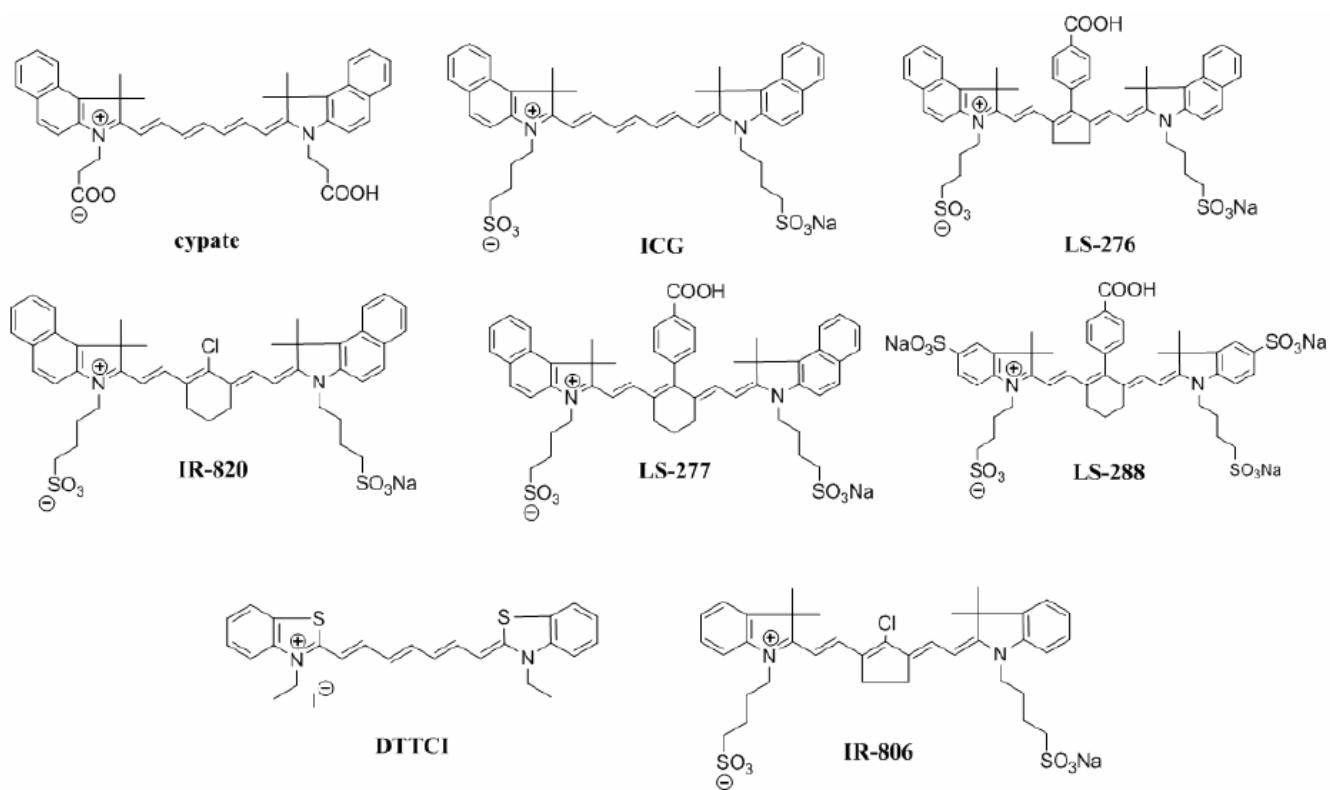


**Fig. 1.**  
Chemical structures of NIR fluorescent dyes used in this study.

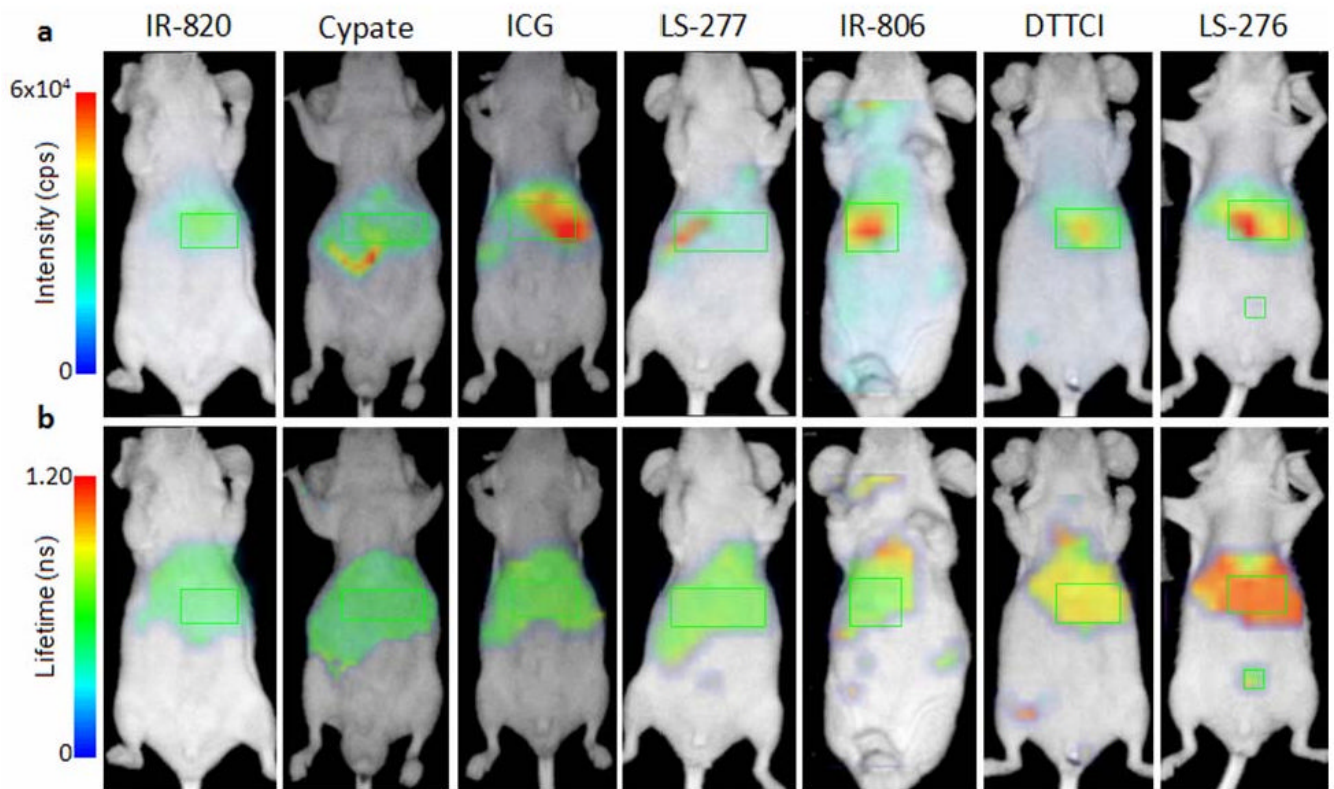


**Fig. 2.**

In vivo fluorescence intensity (a) and FLT (b) ventral aspect image maps of mice injected with NIR fluorescent dyes 1-4 hours post-injection. FLT maps were created from TPSF data acquired using the time-domain diffuse optical imaging system. FLT measurements were selected from the liver region (green rectangles) based on high fluorescence intensity and anatomical location for comparison to minimize discrepancies in organ distribution as all dyes showed evidence of hepatobiliary elimination. Some of the dyes showed partial renal clearance with fluorescence signal from the bladder (indicated by abdominal ROI for LS-276). Collected signal was insufficient for accurate FLT measurement from the bladder for the above specimens. Differences in the positions of the liver and kidney regions in different animals are due to the shifting of these internal organs in animals.

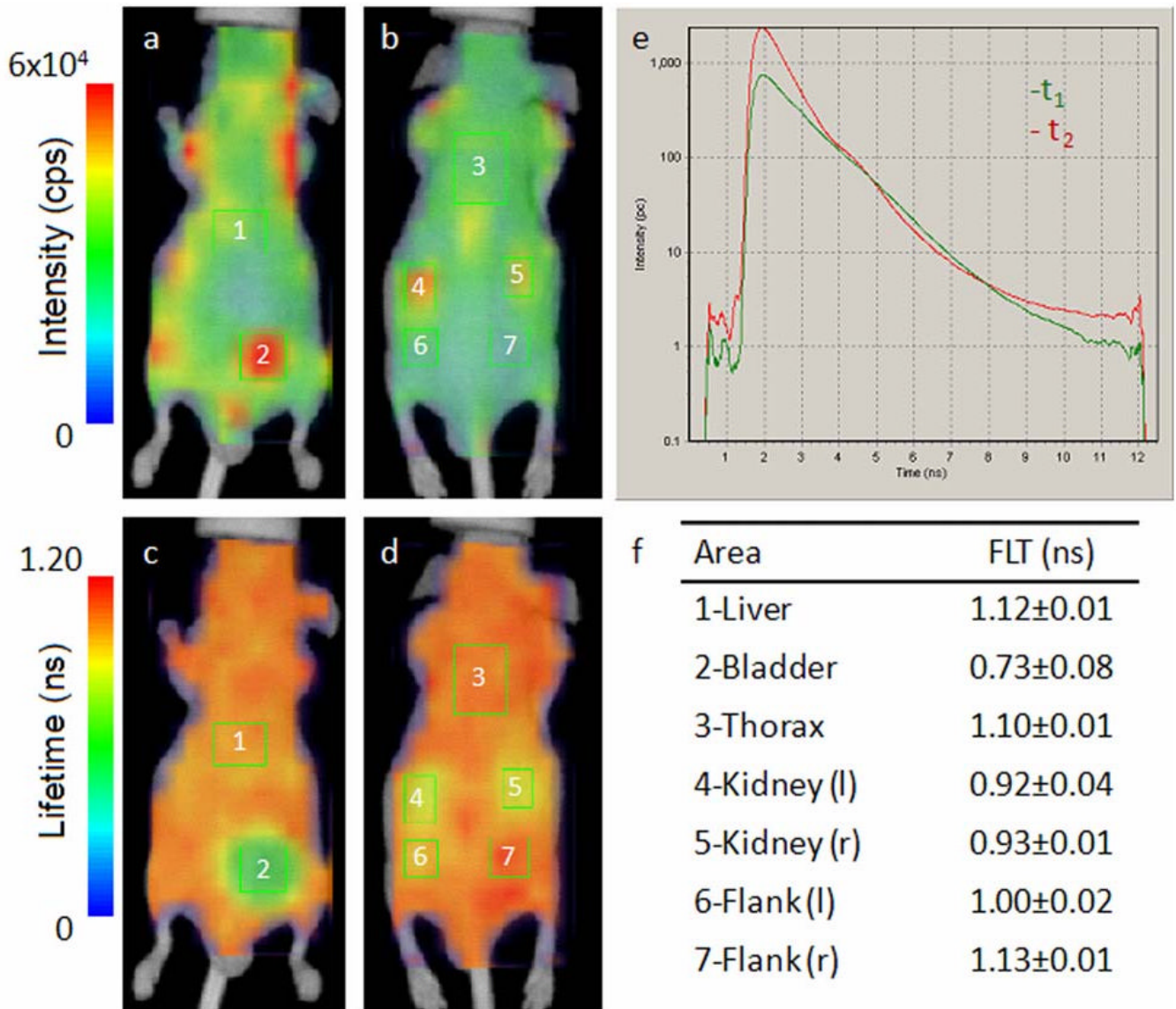


**Fig. 3.**

In vivo fluorescence intensity (ventral (a) and dorsal (b)) and FLT maps (ventral (c) and dorsal (d)) of nude mouse after 2 hours intravenous injection of LS-288 solution. The FLT distribution is heterogeneous with distinctly different FLT values observed in the bladder and kidneys relative to the rest of the body. Representative fluorescence TPSFs for the liver (1) and bladder (2) regions of interest (ROIs) are shown in (e) and demonstrate the dominance of the long-FLT component in the liver and the short-FLT component in the bladder (multiexponential fitting data in Table 2.) The mean detected FLT from each ROI is presented in (f), which compares favorably with the expected water-rich environment in urine. ROI 6 corresponds to the dorsal aspect of ROI 2 (bladder), indicating that the short FLT relative to ROI 7 is due to muscle tissue overlying ROI 2 in this position. A tomographic method could be used to isolate the contribution of adjacent tissues to the FLT.

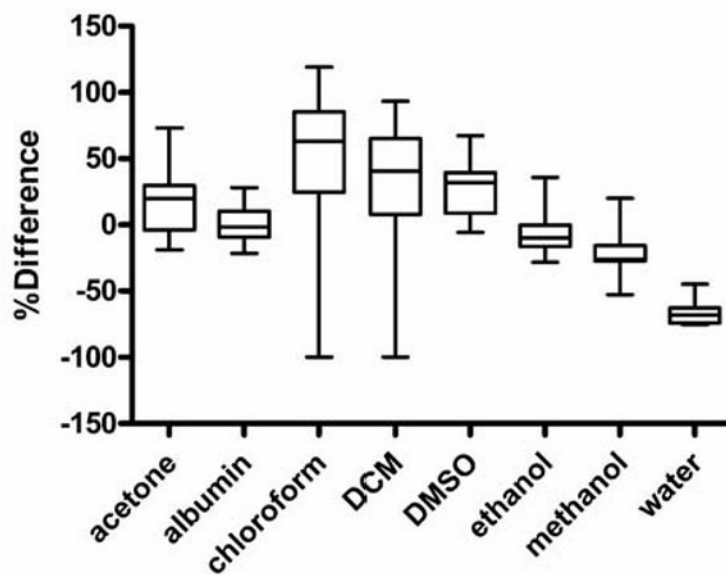


**Fig. 4.**

Box and whiskers plot of FLTs measured in various solvents and referenced to in vivo data from liver regions. The mean percent difference for fluorescence lifetimes for the dyes measured in albumin solution is close to 0 (0.7%), indicating good agreement between the two systems. The maximum difference for albumin was 28% with median difference of 2%. All of the other systems showed median difference of 10% or greater. The largest mean differences between the in vivo and albumin models were observed for DTTCl (28%) and LS-276 (21%). These differences appear to be related to the protein binding fractions as shown in Table 2.

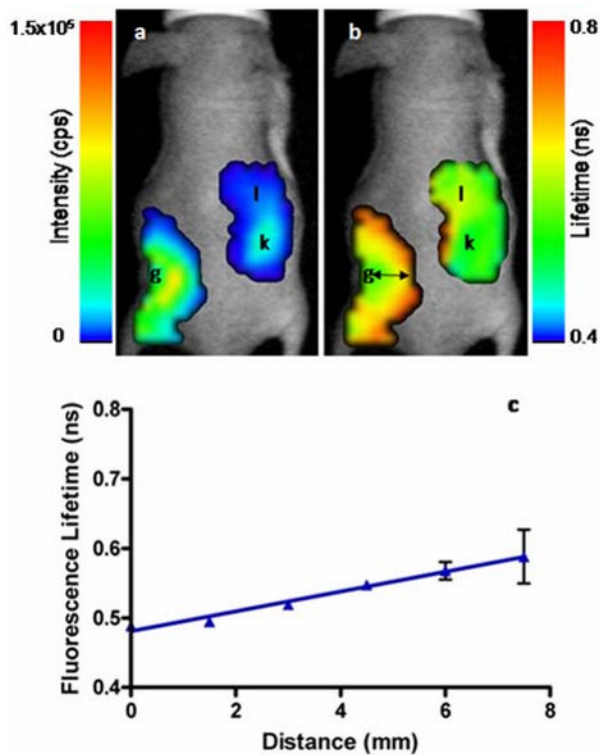


**Fig. 5.** In vivo fluorescence intensity (a) and FLT (b) maps of a mouse 3 hours after subcutaneous implantation of cypate-loaded agarose gel (g). The FLT of cypate increased as it diffused through the subcutaneous space from the gel and was absorbed into the blood. Fluorescence can be seen in the right kidney (k) and the liver (l) regions with distinctly different FLTs consistent with the dye environment. A plot of FLT (b) at distances from the agarose gel (black arrows) demonstrates the difference in cypate FLT as it diffused from the gel.

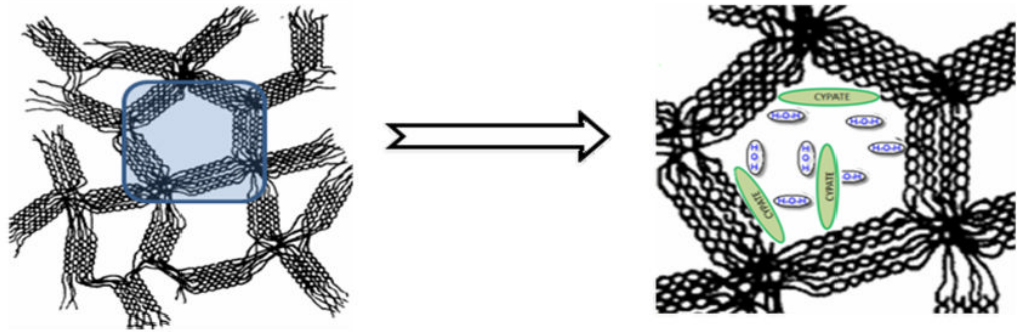


**Fig. 6.** 3D gel structure of agarose (adopted with permission from *J. Mol. Biol.* 1974, 90, 269-284).  
<sup>33</sup> Microcavities are filled with water molecules (more than 99% of the mass of the gel is water).



Table 1

FLTs (ns) of NIR molecular probes measured in various solvents and after intravenous administration in living mice. Data were fitted by a single exponential decay model. Standard deviations (sd) were less than 5% for *in vitro* measurements.

	chloroform	DCM <sup>a</sup>	DMSO <sup>b</sup>	acetone	ethanol	methanol	water	albumin	in vivo±sd
LS-288	N/A <sup>c</sup>	N/A	1.33	1.02	1.00	0.81	0.44	1.00	1.12±0.02
LS-276	1.25	1.17	1.11	1.13	0.87	0.83	0.36	0.88	1.12±0.01
DTTCI	1.82	1.72	1.49	1.54	1.21	1.07	0.49	1.14	1.04±0.01
IR-806	1.28	1.15	1.01	1.02	0.82	0.66	0.27	0.61	0.77±0.02
LS-277	1.62	1.34	0.98	0.84	0.69	0.61	0.2	0.78	0.74±0.00
ICG	1.14	0.91	0.97	0.87	0.62	0.51	0.17	0.79	0.69±0.01
Cypate	1.01	0.94	0.87	0.8	0.57	0.46	0.2	0.62	0.63±0.00
IR-820	0.73	0.59	0.50	0.43	0.38	0.25	0.13	0.49	0.53±0.02

<sup>a</sup>DCM, dichloromethane;

<sup>b</sup>DMSO, dimethylsulfoxide;

<sup>c</sup>N/A, not applicable

**Table 2**

Measured two-component FLT ( $\tau$ , ns) of dyes from albumin solutions compared with FLTs in the liver region in mice after intravenous administration. Good agreement was observed between the two FLT components in vitro and in vivo. The in vitro and in vivo fractional composition of FLTs in the liver were significantly different for LS-276 and DTTCI, indicating the differences in protein-binding characteristics of the molecular probes. Standard deviations for in vitro measurements were less than 5%.

Compound	<i>in vitro</i>		<i>in vivo</i>	
	$\tau_1$ (F <sub>1</sub> ) <sup>a</sup>	$\tau_2$ (F <sub>2</sub> )	$\tau_1$ (F <sub>1</sub> )	$\tau_2$ (F <sub>2</sub> )
LS-276	0.69 (55)	1.19 (42)	0.77±0.06 (14)	1.16±0.02 (86)
DTTCI	NS <sup>b</sup>	1.14 (95)	0.34±0.03 (30)	1.12±0.02 (70)
IR-806	0.52 (60)	1.19 (38)	0.45±0.02 (62)	1.04±0.04 (38)
LS-277	0.64 (65)	1.15 (32)	0.48±0.03 (63)	0.98±0.02 (37)
Cypate	0.47 (69)	0.97 (30)	0.41±0.01 (75)	0.96±0.01 (25)
ICG	0.63 (61)	1.10 (37)	0.53±0.02 (67)	0.90±0.02 (33)
IR-820	0.41 (77)	0.91 (19)	0.41±0.02 (85)	0.92±0.02 (15)

<sup>a</sup>Fractional component (%);

<sup>b</sup>NS, not significant

Measured FLTs ( $\tau$ , ns) of LS-288 in vitro and in vivo comparing the protein-bound fractions in albumin solution and in the liver ROI to that of relatively water-rich urine. Standard deviations were less than 5% for in vitro measurements.

**Table 3**

	in vitro		in vivo	
	$\tau_1$ ( $F_1$ )	$\tau_2$ ( $F_2$ )	$\tau_1$ ( $F_1$ )	$\tau_2$ ( $F_2$ )
Albumin	0.61 (37)	1.29 (60)	0.65±0.06 (29)	1.23±0.03 (71)
Urine	0.42 (82)	0.99 (15)	0.48±0.02 (75)	1.09±0.05 (25)